THERMOSENSE 2005
(Part of SPIE's International Symposium on Defense and Security)

Simultaneous Visible And Thermal Imaging Of Metals During Machining

Eric Whitenton, Robert Ivester, Howard Yoon
National Institute of Standards and Technology, Gaithersburg MD 20899, USA

ABSTRACT

In order to investigate temperatures reached during orthogonal metal cutting, a novel approach for measuring temperatures at the tool-chip interface has been developed based on high-speed thermography. A thermal infrared camera and a visible camera combined through a dichroic beam splitter form the basis for a synchronized visible and infrared imaging system. Pairing the infrared camera with a higher speed visible camera allows for assessment of thermal images with aberrant chip flow or an obstructed view of the tool/chip interface. This feature facilitates the use of the apparatus in machining environments where machining chips or other debris fly about. The measurement setup also includes a force dynamometer, custom timing circuitry, and a high-speed digital oscilloscope to enable timing of frames together with force measurements so that analysis of the infrared images can be compared against the energy levels measured through the cutting forces. The resulting infrared images were converted to radiance temperatures through comparison to a NIST calibrated blackbody. Emissivity was measured by thermally imaging the machining chips heated to known temperatures. Machining experiments were performed at various cutting speeds and at two different infrared wavelengths. Analysis of these experiments gives insight into the relationships between emissivity, temperature, surface condition, infrared wavelength and motion blur. The analysis shows that using the visible, thermal and force data together is a significant improvement over any of these alone. These insights lead to practical guidance for use of infrared imaging systems to image rapidly moving objects.

KEYWORDS

Metal cutting, high-speed video, thermal spectrum video, data synchronization, image processing, motion blur.

1. INTRODUCTION

To study the machining process it is important to accurately measure the temperatures produced. These temperatures are used in two ways. First, thermal data is used as input into machining models. Second, measured temperature data can be used to validate models predicting temperature. There are several techniques available for performing this measurement. Thermal imaging was the method chosen for use in a study[1] of orthogonal metal cutting at NIST. However, it was soon realized that a thermal camera alone did not always give accurate data. Machining chips move at high velocities causing significant motion blur in the thermal images. Also, chips can flow in unexpected directions, which degrade the thermal images. Examples of both of these issues will be presented in this paper. The primary focus of this paper is on the techniques and the issues arising in such measurements. Specifics of particular machining experiments are presented only as examples. Recommendations for the thermal imaging of machining when simultaneous high-speed visible light imaging is not an option are also briefly discussed.

Disclaimer: Commercial equipment and materials are identified in order to adequately specify certain procedures. In no case does such identification imply recommendation or endorsement by the National Institute of Standards and Technology, nor does it imply that the materials or equipment identified are necessarily the best available for the purpose.

2. EXPERIMENTAL SETUP

A simultaneous synchronized visible and thermal imaging system was constructed using a thermal infrared camera and a visible camera combined with a dichroic beam splitter. Figure 1 shows a schematic diagram of the optics and machine tool hardware. Figure 2 shows a close-up photograph. Since the primary 15x lens must gather both visible and infrared light, it is a reflective optic. All other optics used in the system are refractive. The light then passes through a dichroic beam splitter, which separates the visible wavelengths from the infrared, and sends each toward the appropriate camera. In the visible light leg of the optical path, there is a conventional beam splitter to facilitate through-the-lens lighting. Even though they share a common primary lens, the effective magnifications need not be the same for the two cameras. The power of the collector lens for each camera may be chosen individually to effect the magnifications independently. The magnification of both the visible and thermal cameras, as well as the registry between their images, was determined by imaging resolution targets and precision pinholes.

Both the visible light and the thermal spectrum camera are capable of a maximum possible frame rate and a shortest possible integration time (shutter time). However, various constraints, such as the amount of radiation reflected or emitted, place bounds on the frame rates and integration times achieved in practice. The visible light camera is capable of up to 120000 frames per second (fps), however, 6000 fps is more typical. The shortest integration time possible is 4.2 µs, with a typical speed of 167 µs. The thermal camera is capable of up to 3000 fps, with a typical setting of 150 fps. The shortest integration time is 6 µs, but a typical integration time is 1500 µs.

The measurement setup also includes a 3-axis force dynamometer, custom timing circuitry, and a high-speed digital oscilloscope. This enables timing of frames together with force measurements so that analysis of the infrared images can be coupled with and compared against the energy levels measured through the cutting forces. The workpiece is cylindrical tube with a diameter of approximately 101 mm bolted to the spindle faceplate. The tool is plunged into the end of the rotating tube to perform the orthogonal cut.

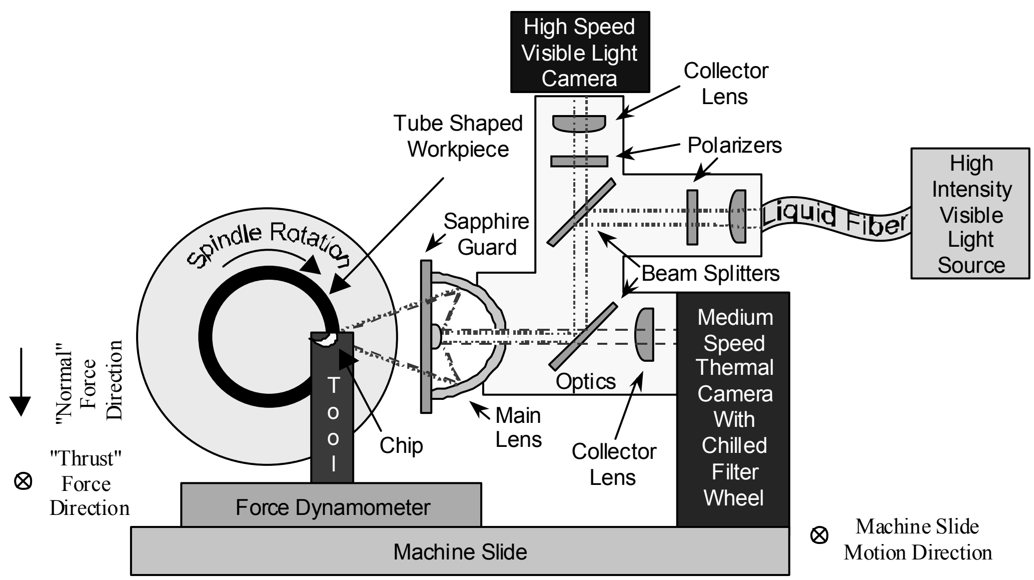

Figure 1: Schematic of the experimental setup.

3. CAMERA CALIBRATION

The resulting infrared images were converted to temperatures using two NIST traceable calibrated blackbodies, one with a maximum temperature of 150 °C and the other with a maximum temperature of 1100 °C. An automated system takes a sequence of blackbody images and combines them into a database. Interpolation of the data base information is used to convert camera readings of the machining process to spectral radiance temperatures. Wien's law[2] and emissivity data are then used to convert spectral radiance temperatures into thermodynamic temperatures, sometimes referred to as "true" temperatures. This is shown in Equation 1, where T_s and T_l denote the true temperature in Kelvin and spectral radiance temperature in Kelvin, λ represents the mean spectral wavelength, c_2=14387 µm·K is the second radiation constant, and e_λ is the emissivity at the spectral wavelength.

$$1/ T_s = (1/ T_l) + (\lambda \,*\ln(e_\lambda) / c_2) \qquad (1)$$

4. EMISSIVITY MEASUREMENTS

The reflectance of an AL7075-T651 aluminum workpiece was measured as a function of wavelength[3]. This is shown in Figure 3. Since emissivity equals one minus reflectance, this can be used to estimate the emissivity of the work piece to be 0.045 with an expanded uncertainty of ± 0.005 (k=2)[4] at room temperature in the 3 µm to 5 µm wavelength range.

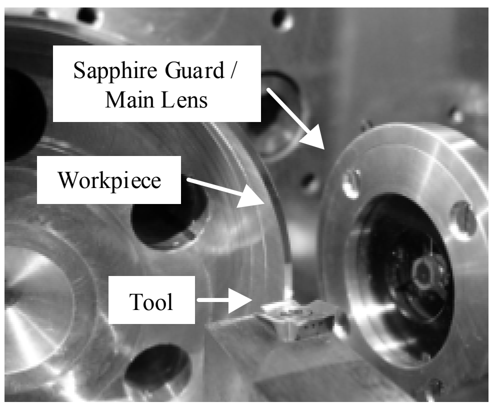

Figure 2: Close-up photo of experimental setup.

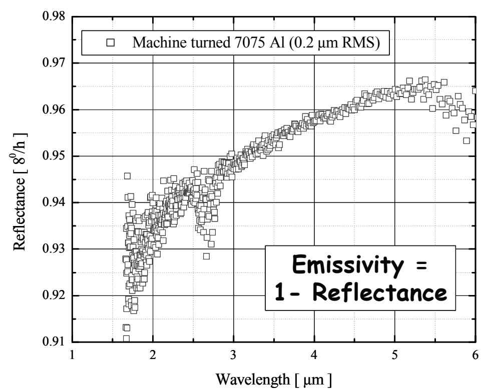

Figure 3: Reflectance vs. wavelength of the aluminum work piece.

However, the surface texture of the machining chips is significantly rougher than that of the workpiece, so emissivity is expected to be higher. The chips are too small to be used in the reflectivity measuring device used above, so an alternate method of estimating the emissivity was used. Pieces of the chips, along with a thermocouple sandwiched between the chips, were clamped together in a pin vice. They were then heated by passing an electric current through the pin vice and imaged with the camera system. This is shown in Figures 4 and 5. The chips are approximately 0.15 mm thick. To ensure that there is no reflection of the hot pin vice on the edge of the chips, the chips and thermocouple protrude out of the pin vice by approximately 1 mm. The pin vice is therefore expected to be hotter than the chips. However, since the thermocouple is in direct contact with the chips, the thermocouple temperature is expected to be close to that of the chips. Two examples are shown in Figure 6.

If differences between the thermocouple temperature and measured chip temperatures are attributed to variations in the emissivity across the chip surface, then emissivity maps may be calculated and histograms of the emissivities plotted. Since several chip sections were examined at several temperatures, multiple histograms were generated. Shown in Figure 7, a mean value may be computed for each histogram, and the mean of those means computed. This mean of the means is 0.345 with an expanded uncertainty of ± 0.05 (k=2)[4] in the 275 °C to 575 °C temperature range. As expected due to the change in surface roughness, the values of emissivities we attained for the chips are significantly higher than for the workpiece. While the variation in emissivity is large, there is significant motion blur in the thermal images and so the variations in emissivity are not actually seen in those images. Thus, the mean of the means value works well. For example, a typical integration time for the thermal images is 1.5 ms. During that time, depending on the cutting velocity, 65 mm to 180 mm of chip length passes through the 0.24 mm field of view.

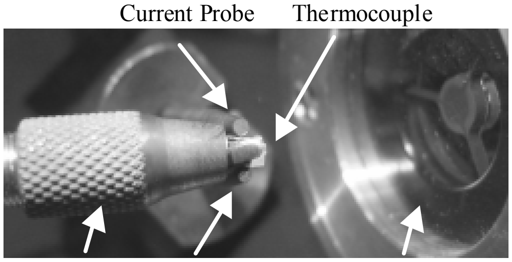

Figure 4: Apparatus for imaging the edges of the machining chips at elevated temperatures.

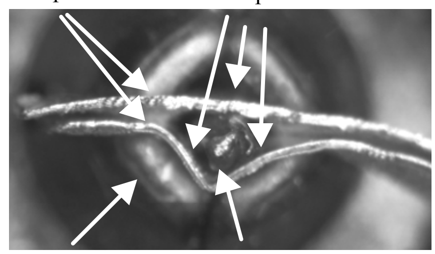

Figure 5: Close-up of the thermocouple sandwiched between 2 aluminum chips held in a pin vice. The chips are approximately 0.15 mm thick..

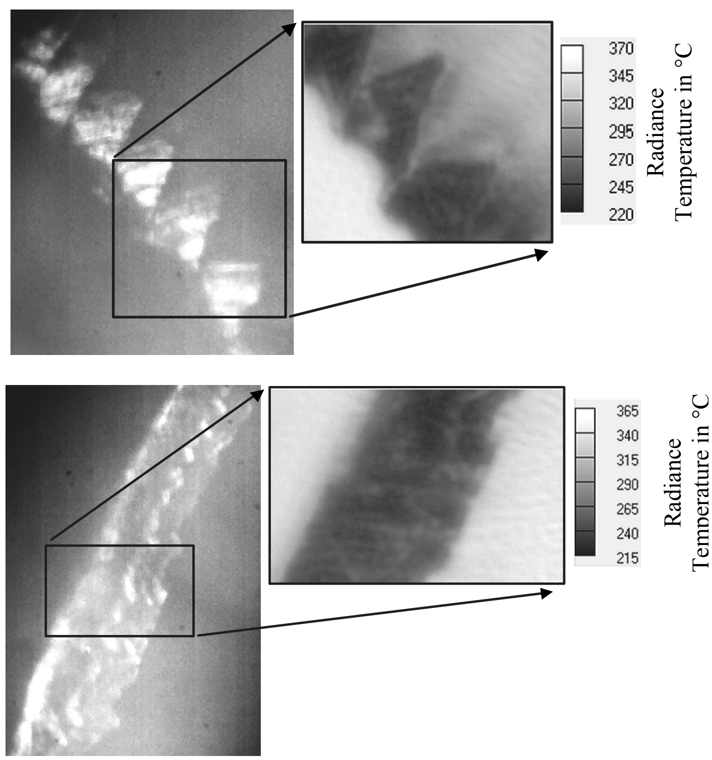

Figure 6: Visible light images (left) and thermal images (right) of heated chips. The top set of images shows a serrated chip while the bottom shows a more typical uniform chip. The chips are approximately 0.15 mm thick. Temperatures are radiance temperatures.

5. ANALYSIS OF MACHINING EXPERIMENTS

5.1 Components of a machining experiment image

Figure 8 shows a schematic diagram of a typical visible or thermal image. There are 3 areas of potential interest to a researcher; the workpiece, the tool and the chip. There are 3 broad lines separating these areas. These lines may also be of interest. The line separating the chip and the workpiece is called the cutting zone. The line separating the tool and the workpiece is called the clearance face. The line separating the tool and the chip is called the rake face or the chip/tool interface.

The cutting zone is where the bulk of material deformation occurs. The emissivity of this area changes from that of the workpiece to that of the chip. In Section 4 we showed that the workpiece and the chip can have very different emissivities. With such a wide variation in the emissivities in this portion of the image, the level of uncertainty in the temperature measurement is therefore inherently high. The workpiece is typically close to room temperature, which is significantly cooler than the cutting zone. Because of the limited dynamic range in the sensitivity of the thermal camera, a setting (integration time and filter used) which accurately captures the very hot cutting zone does not accurately capture the workpiece temperature. Also, since the cutting zone emits significantly more infrared than the workpiece, one must be careful to avoid veiling glare[5] and other effects causing errors in the workpiece temperature measurement. The temperature of the tool is not difficult to measure if you have measured the tool's emissivity. However, as will be shown later in this paper, it is problematic to measure it and the chip temperature simultaneously. The clearance face of the tool is difficult to interpret. This is because there is often a gap between the tool and the workpiece in this region of the image. This gap often acts like a micro-blackbody with a much higher emissivity than either the tool or the workpiece. The friction between the chip and the tool causes the chip/tool interface to be the hottest portion of the chip. In many materials, this frictional heat can cause cratering of the tool, shortening the tool's useful life. The chip/tool interface is the portion of the image we analyze in this paper.

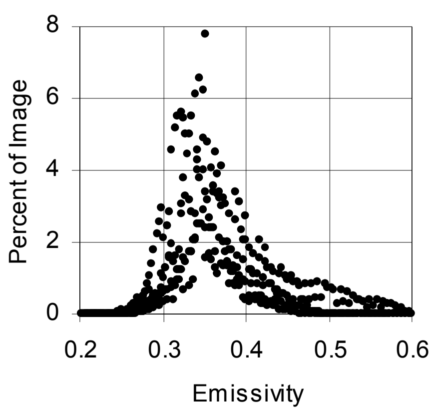

Figure 7: Multiple histograms of chip emissivity measurements.

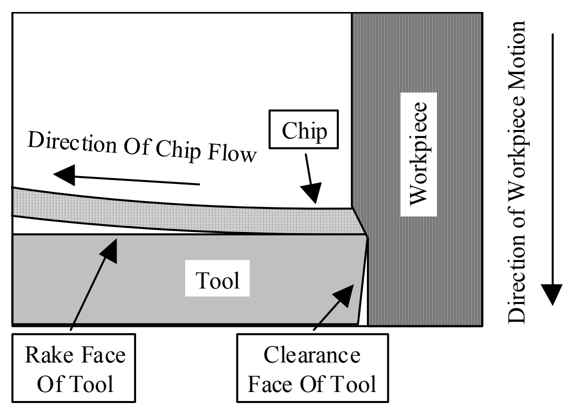

Figure 8: Schematic of an image of a machining experiment.

5.2 Controlling what is imaged

As shown in Figure 9, understanding and controlling what is actually being imaged is very important for accurate interpretation. Any optical system has some limit on the depth of focus. This fact may be used to control what is being measured. In Scenario 1, only the chip and the chip/tool interface are in focus. In Scenario 2, the side of the tool is in focus as well. In theory, the advantage with Scenario 2 is that temperatures of both the body of the tool as well as that of the chip/tool interface may be measured. However, the tool is only a pixel or two away from the chip/tool interface in the image. Real machine tools move, thermally expand and vibrate, which causes the position of the tool in the images to vary somewhat from frame to frame. The chip position, and the chip/tool interface position, varies with time because the chip itself is shifting laterally and vertically with time. The emissivity of the tool is higher than that of the chip, and appears brighter than the chip. These factors work together to cause three potential problems. 1) In any optical camera system, very bright pixels have some effect on the darker ones[5]. The close proximity of the chip/tool interface and the tool may allow the brighter tool to affect the chip/tool interface temperature measurement. 2) Since the exact location of the chip/tool interface varies from frame to frame, it must be determined on a per frame basis. 3) Any error in the estimate of the chip/tool interface position results in large errors in the chip/tool interface temperature measurement. Scenario 1 virtually eliminates problems 1 and 3, and makes solving problem 2 trivial. This approach will be explored later in this paper.

5.3 Factors that can cause aberrant thermal images

Machining is a dynamic and often erratic process. There are many factors that can make a thermal image unsuitable for determining a temperature. 1) The width of the chip changes during the cutting process. Due to the difference in the wavelengths of light, thermal images have a broader depth of focus than the visible images. However, if the chip is sufficiently out of focus, then the infrared camera captures less of the emitted radiation and the resulting temperature measurements will be negatively biased (too low). 2) Figure 10 shows a lump of material that has built up on the cutting edge of the tool forcing the chip to flow over it. This built up edge, or BUE, can create a gap between the chip and the tool that can behave like a micro-blackbody. If not taken into account, the higher than expected effective emissivity of the gap results in the temperatures measured being positively biased (too high). 3) Chips often fly off in random directions. A flying chip that comes between the lens and the chip being imaged can cause the temperature estimates to be either positively or negatively biased. 4) A flying chip may also come between the lens and the chip being imaged, but be outside the camera's field of view. In the visible spectrum, light can reflect off this flying chip and cause odd looking bright spots in the image. In the thermal spectrum, this flying chip is sometimes hot enough to act as a light source that may reflect off the chip being imaged. This positively biases the thermal measurements. 5) A lip or burr can sometimes form on the edge of the workpiece and partially obscure the view, resulting in a negative bias. 6) In Figure 11, the effect of "pig tails" on thermal images is shown. A pig tail is when material flows towards the camera, perpendicular to the chip flow direction. Its speed is much slower than that of the chip, and often occurs when the tool is worn. The upper visible/thermal image pair shows a good radiance temperature measurement of the chip/tool interface. The presence of a pig tail is obvious in the center thermal image but not obvious at all in the lower thermal image without the accompanying visible light image. Note the 35 °C difference between the top (good) and the bottom (aberrant) thermal images.

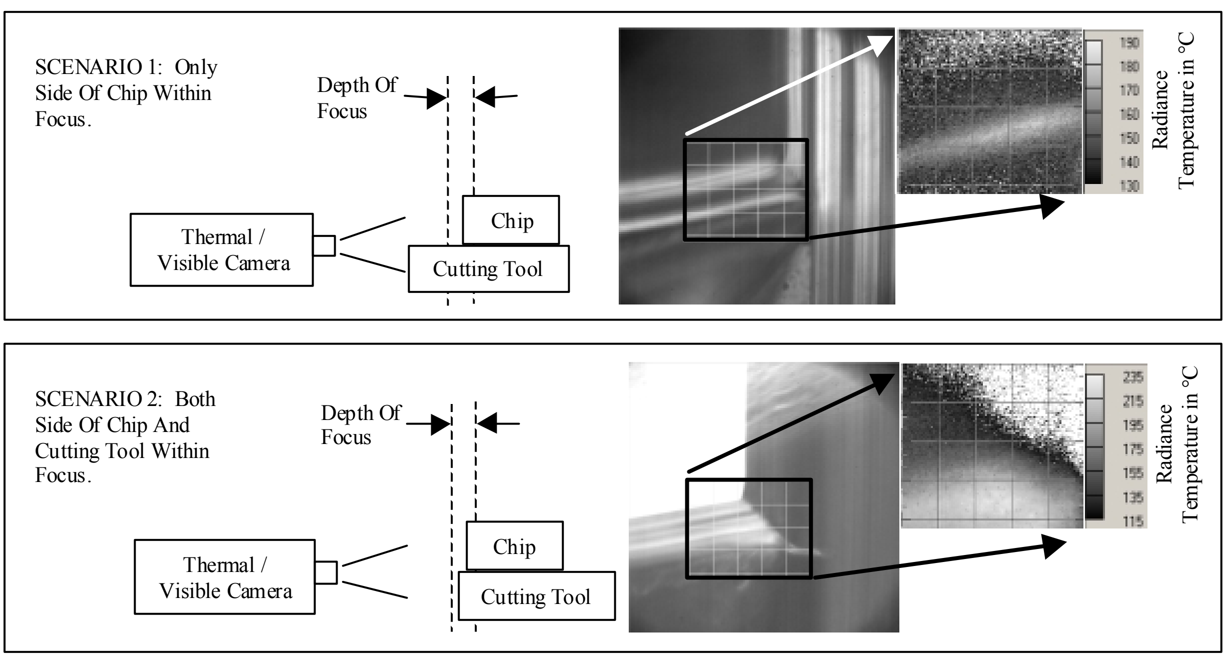

Figure 9: Visible light images (left) and thermal images (right). The width of the field of view is 520 µm for the visible light and 240 µm for the thermal images. The rake angle of the tool is + 15 degrees. Temperatures shown are radiance temperatures.

5.4 Successful determination of the temperature profile along the rake face

Many images are aberrant and must be ignored. One approach is to look at only the thermal images to determine which are aberrant. However, as shown above, there are times when it is not obvious from thermal images alone that those images are bad. For example, if a temperature appears to fluctuate from one thermal image to the next, that fluctuation may be caused by cyclic behavior in the machining dynamics, or it may be caused by aberrant images giving the appearance of cyclic behavior. From a measurement point of view, judging the quality of data solely by the data alone is problematic. Whenever possible, independent verification should be sought.

The higher frame rate, shorter integration time, and better resolution of visible images, when paired with thermal images, allows for more reliable verification and classification of thermal images. This process is automated as follows. First, a visible light image judged to be a “clean” image is selected by the operator as a reference image. Next, a computer program compares each image in the visible light movie to the selected reference image. For each visible light image determined to be sufficiently like the reference, the matching thermal image is marked “good”. All other thermal images are considered aberrant. This generally did a good job of sifting out aberrant thermal images. On occasion, however, an aberrant thermal image made its way through the filter and had to be removed manually. Generally, this corresponded to a bad visible light image occurring a few frames before the frame in question. This is sensible – if a BUE forms and is subsequently swept away, for example, the machining process will take some amount of time to re-equilibrate to a steady state temperature. Future versions of the software will require not only the current frame to be like the reference image, but some number of the preceding frames to be like the reference image as well.

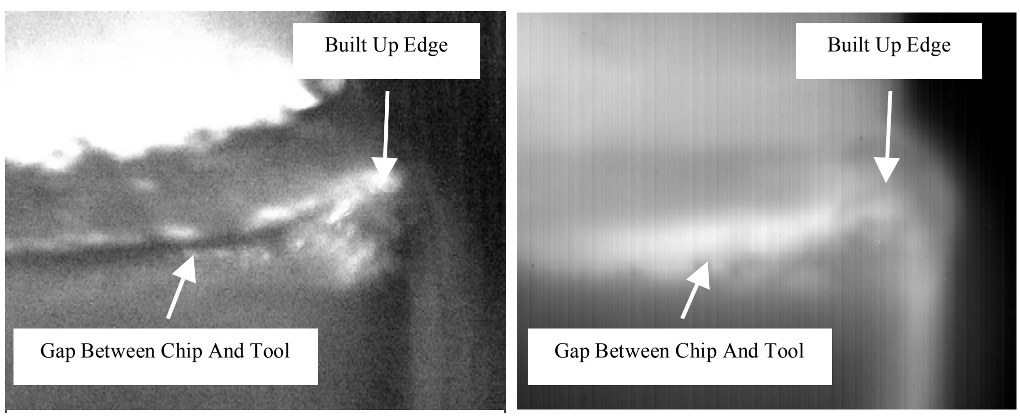

Visible Light Camera View

Unprocessed Thermal Camera View

Figure 10: Gap between the tool and the rake face causes unexpected emissivity issues. The rake face angle is approximately 0 degrees.

There are many possible algorithms for performing image comparisons[6]. The concept behind the algorithm we used is to compare each image to a reference image in a variety of ways and allow each of those comparisons to cast a vote as to whether or not the images are alike. The frames receiving the most votes are selected as good. This approach allows both multiple reference images and multiple types of statistical comparisons to be used. Using multiple comparison statistics and reference images enhances the robustness of the algorithm because if one type of comparison statistic happens to be fooled by an odd image, it will simply be out voted by the other statistics. In the current version of our software, different statistical comparisons are achieved by applying various image transforms to the images before a sum of absolute differences between the transformed images is computed. We are currently using 4 transformations - as is, average removed, best fit plane removed, best fit plane removed then normalized by 1/standard deviation. These transformations were selected because they tend to correct for different overall lighting conditions in the images. More sophisticated transformations such as Fast Fourier Transform could be added, but these generally take longer to execute. The transforms selected performed adequately. The algorithm is shown in Figure 12.

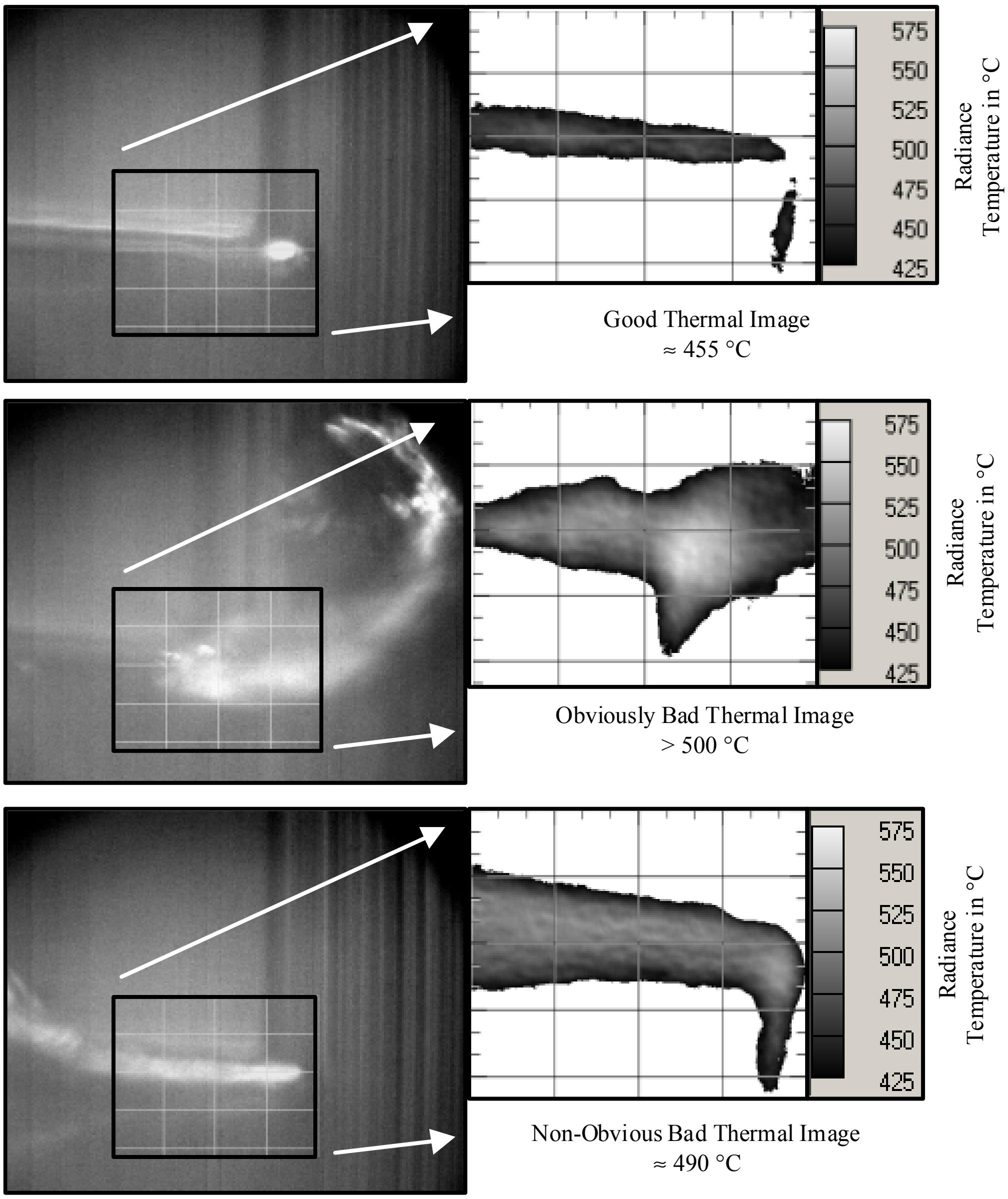

Figure 11: How "pig tails" can potentially produce errors in temperature measurement. The upper visible/thermal image pair shows a good radiance temperature measurement of the chip/tool interface (the rake face). The presence of a pig tail is obvious in the center thermal image but not obvious in the lower thermal image without the accompanying visible light image. Note the 35 °C difference between the top (good) and the bottom (aberrant) images. The field of view width for the visible light images are 520 µm. The field of view width for the thermal images is 240 µm. The rake face angle is approximately 0 degrees. Temperatures shown are radiance temperatures.

Now, we consider determining the chip/tool interface temperature from the thermal images. We will analyze images from Scenario 1 type tests (see Figure 9). If we simply selected the highest value from the thermal image, the results would be sensitive to noise in the thermal images. Also, we want to ignore the clearance face temperature for this measurement. Thus, some form of image processing is required. Our procedure is shown in Figure 13. Once the peak temperatures have been determined from the thermal frames, they are converted from radiance temperatures to temperatures as discussed in Section 3.

Figures 14 and 15 show data for Scenario 1 type tests of aluminum workpieces. The force data are shown here for completeness, and discussed in Ivester[1]. The small dots represent peak temperatures of aberrant thermal images. The large dots are the peak temperatures of the good thermal images. In Figure 14, the results for 2 different thermal camera wavelengths are compared. In Figure 15, two cutting speeds are compared. Note how the temperatures from the good thermal images rise to a plateau, while the aberrant thermal images fluctuate wildly. If, for each test condition, we average the temperatures from the good thermal images occurring after 0.5 s, we may compute a plateau temperature for each test condition. Shown in Figure 16, the error bars show the uncertainty resulting from the uncertainty in the emissivity as discussed in Section 4.

6. DETERMINING IF A SIMULTANEOUS VISIBLE AND THERMAL IMAGING SYSTEM IS NEEDED

While the simultaneous visible and thermal imaging system is a very powerful tool, it is also an expensive and somewhat complicated one. For “ill behaved” machining processes, it is the only technique we are aware of that adequately deals with many of the problems. However, one may make the case that a particular set of cutting conditions and materials are well behaved and, therefore, do not require this level of sophistication. How do you really know if a cutting process is in fact well behaved? We recommend the following relatively low cost solution.
Figure 17 shows a conventional camcorder used to image the chips through a macro lens or a microscope lens attachment. The video output is converted to a once per frame pulse using a video signal converter purchased from a video equipment supply house. The once per frame pulse triggers an inexpensive strobe/tachometer unit commonly used in machine shops. The room lights need to be off or the machine needs to be covered so that the only light the camcorder sees is that of the strobe. When set up properly, this system outputs a surprisingly good quality movie. While the frame rate is far too low to study chip dynamics, if the entire range of cutting conditions of interest are imaged with this setup, and all of the images look good, then the thermal images will likely be good as well. If not, the thermal images may be suspect.

7. CONCLUSIONS

When characterizing the machining process, having the visible, thermal and force data together is a significant improvement over any of these alone. This paper examined many of the issues and sources of error which may occur, and has shown that many of these may be overcome by intelligent use of this technique. However, we also showed how one may easily determine if the cutting process is well behaved enough to justify the simpler and less costly method of thermal imaging alone.

ACKNOWLEDGEMENTS

The authors wish to acknowledge M. Davies, A. Cooke, T. Raines, A. Skaggs, C. Higgins, L. Deshayes, B. Ayres, B. Dutterer and M. Huff for their contributions in designing, implementing and analyzing the experiments.

Each frame has its own vote counter. Initialize them to zero.

For each type of statistical comparison (currently 4 of them) do:

> *For each reference image (generally 1 of them) do:*
>
> > *Create a list where each frame in the movie produces 1 item in the list. Each item in the list is a {frame number, comparison value} pair.*
> >
> > *Sort the list by comparison value so that the best matching frames come to the top of the list.*
> >
> > *For each frame number in the top K1 percent of the list, increment that frame's vote counter by 1. K1 is generally 10 to 25.*
>
> *End do*

End do

The maximum number of votes which may be received by any single frame is the product of the number of comparison statistics and the number of reference images. Mark as good each frame which has received at least K2 percent of the maximum possible votes. K2 is generally 75.

Figure 12: Algorithm for seperating good thermal images from aberrant ones.

For each frame in the thermal movie do:

> *For each X (left to right) location in the frame do:*
>
> > *The temperature as a function of Y (up and down) is fit to a gaussian function. If the quality of the fit is good, and the fit coefficients are within reasonable bounds, a peak temperature is determined from the fit coefficients and is reported for that X location of the thermal frame. If the fit is not a good one, no value is reported, as this generally corresponds to either an aberrant thermal frame or a clearance face temperature, which is a part of the frame we wish to ignore.*
>
> *End do*
>
> *If the frame has sufficient number of reported values, the second highest peak is determined for that frame.*

End do

This results in a maximum temperature as a function of frame number (time) plot. Since not every frame is of sufficient quality to produce a temperature value, the data on the temperature-time plot is unequally spaced in time.

Figure 13: Algorithm for determining the peak temperatures for Scenario 1 type tests.

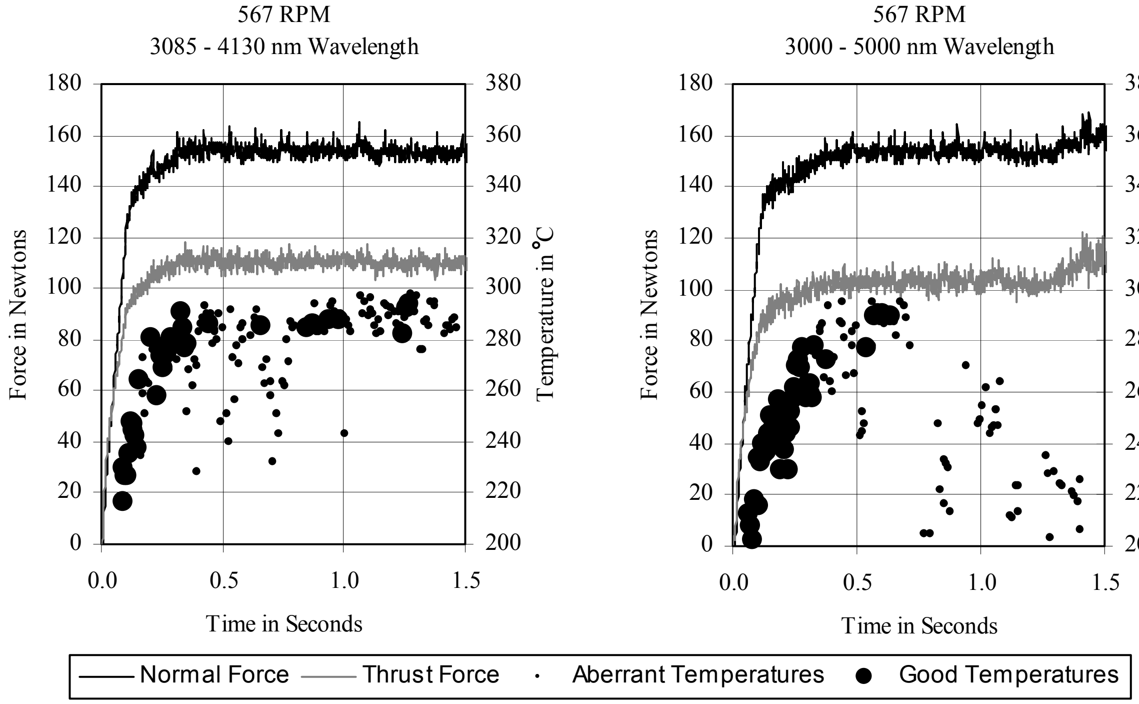

Figure 14: The results for 2 different thermal camera wavelengths are compared. Agreement in the plateau temperature reached in the good thermal images is very good. The rake face angle is 0 degrees.

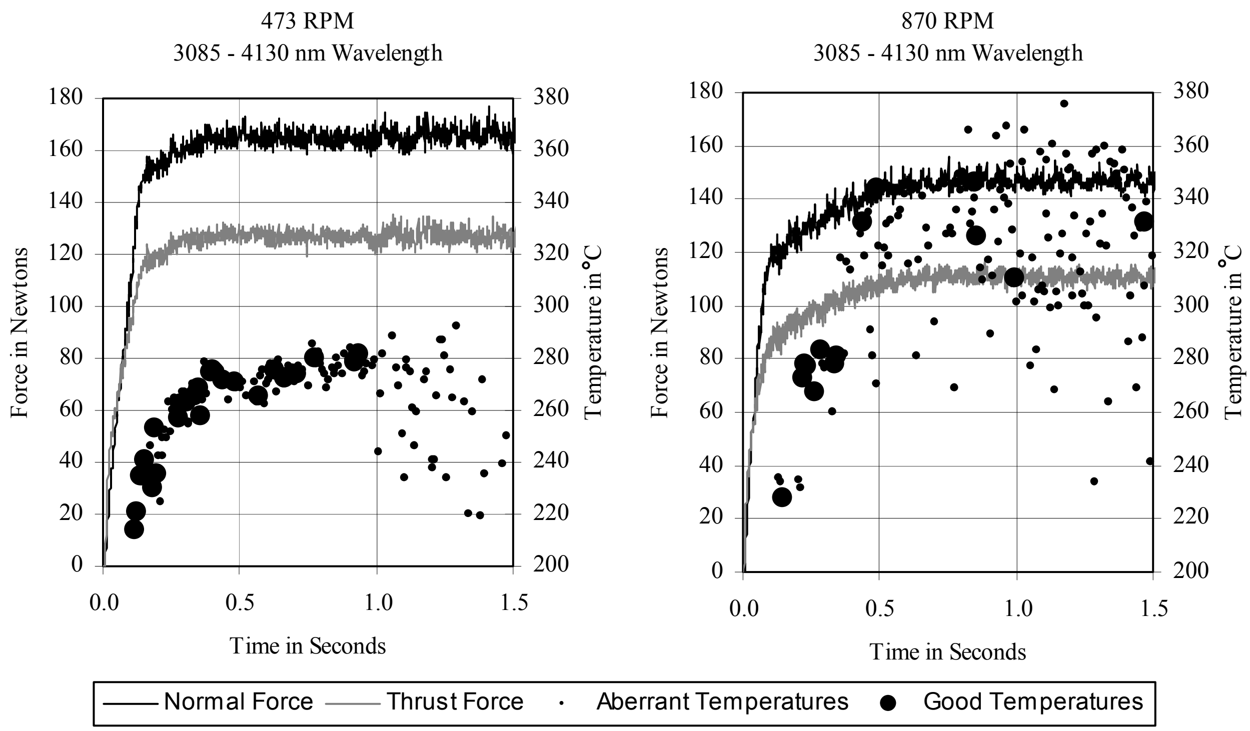

Figure 15: The results for 2 different spindle speeds. As expected, higher cutting speed results in higher plateau temperatures for the good thermal images. The rake face angle is 0 degrees.

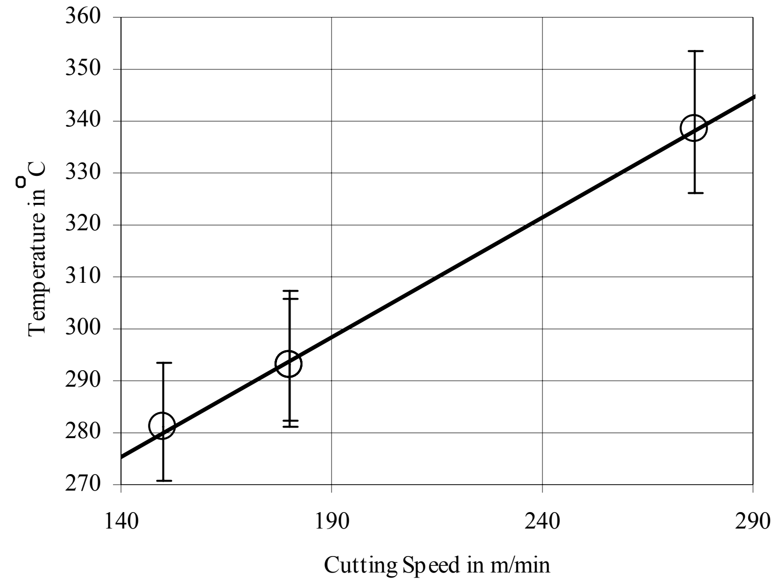

Figure 16: Summarizing the data in Figures 14 and 15. Line is drawn to guide the reader.

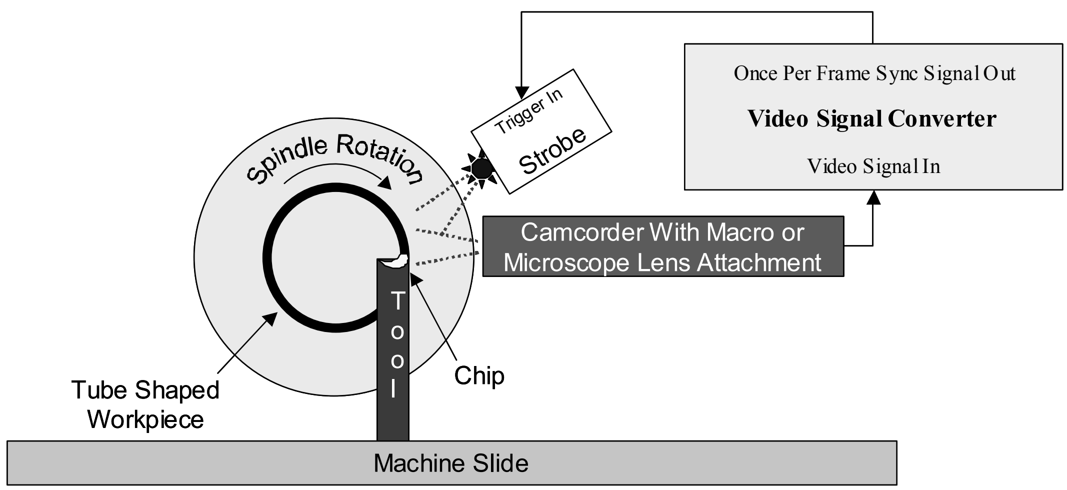

Figure 17: Relatively inexpensive setup to determine if the thermal images are likely to be aberrant.

REFERENCES

1. R. Ivester, E. Whitenton, L. Deshayes, "Comparison Of Measured And Simulated Cutting Temperatures For Machining Of Aluminum", Transactions of the North American Manufacturing Research Institution of SME, Vol.33, 2005.
2. D.P.DeWitt, Gene D. Nutter, *Theory And Practice Of Radiation Thermometry*, John Wiley & Sons, Inc, 1988.
3. S. G. Kaplan and L. M. Hanssen, *Infrared Transmittance Standards 2053, 2054, 2055, and 2056, NIST Special Publication 260-135*, National Institute of Standards and Technology, 2000.
4. Barry N. Taylor, Chris E. Kuyatt, *Guidelines for Evaluating and Expressing the Uncertainty of NIST Measurement Results, NIST Technical Note 1297, 1994 Edition*, National Institute of Standards and Technology, 1994
5. P. A. Boynton, *Evaluation of the Liquid-Filled Camera For Measuring Shadow Detail Part 1: Sensor Evaluation, NIST Internal Report 6900*, National Institute of Standards and Technology, 2002.
6. John C. Russ, *The Image Processing Handbook, Third Edition*, CRC Press, 1999.